On the evolution of a nonlinear, non-hydrostatic internal Kelvin wave in a stratified rotating circular basin

Derek Steinmoeller, Marek Stastna, Kevin Lamb

Department of Applied Mathematics,
University of Waterloo
dsteinmo@math.uwaterloo.ca

Abstract

The evolution of a coastally localized interfacial perturbation propagating in the longshore direction around a two-layer rotating circular basin with a flat bottom is considered. A simple Boussinesq-type reduced gravity shallow water model is used as the equations governing the problem. The equations are recast in polar coordinates and spatially discretized using high-order pseudospectral methods. The effects of nonlinearity and dispersion are studied through a series of numerical simulations. The results are also compared to the geometrically simpler case of a periodic channel. In general, it is found that an undular tail forms behind the initial wavefront due to free Poincaré waves radiating through the interior of the basin and that the formation of this tail can be suppressed by increasing the Coriolis parameter. In strongly nonlinear cases, the wavefront steepens to a near-shock. The formation of a shock is precluded by dispersive effects which redistribute the energy amongst a collection of high-frequency solitary-like waves.

1. Introduction

Much of the biochemical transport and mixing in lakes is strongly influenced by the dynamics of nonlinear internal waves. In this paper, the effects of rotation, dispersion, and nonlinearity on the evolution of an internal Kelvin wave are investigated using a high-order pseudospectral method to solve a weakly non-hydrostatic reduced-gravity shallow water model of Boussinesq-type in a rotating circular basin. The model equations under consideration here are the same as those used by de la Fuente et al. (2008) in their study of the evolution of basin-scale Poincaré and Kelvin waves in a two-layer rotating basin using the finite volume method (FVM). Boussinesq-type models have also previously been used to study dispersive and nonlinear effects in internal waves by Tomasson and Melville (1992). Stocker and Imberger (2003) obtained analytical solutions to the linear rotating shallow water equations in a stratified rotating basin in order to study the evolution of an initial linear interfacial tilt and suddenly imposed constant wind-forcing.

The main contribution of this work is the use of high-order pseudospectral spatial discretization methods that are known to give the best accuracy possible and excellent resolution characteristics (see Boyd (2001) or Trefethen (2000)). Unlike the FVM that imparts inherent numerical dissipation to solutions, pseudospectral methods lack inherent dissipation, and the modeller must specify a small amount of artificial dissipation using a spectral filter in order to stabilize the scheme. We have also opted to focus on the evolution of a localized coastally-propagating interfacial disturbance, similar to a localized linear Kelvin wave, instead of the evolution and break-down of basin-scale waves as done by de la Fuente et al. (2008) and Stocker and Imberger (2003).

2. Methods

The governing equations used by de la Fuente et al. (2008) in their study of internal waves in a circular basin for a single fluid layer are

$$\frac{\partial h}{\partial t} + \nabla \cdot (h\mathbf{u}) = 0\,, \tag{1}$$

$$\frac{\partial (uh)}{\partial t} + \nabla \cdot ((uh)\mathbf{u}) = -g'h\frac{\partial \eta}{\partial x} + fvh + \frac{H^2}{6}\frac{\partial}{\partial x}\left(\nabla \cdot \frac{\partial (\mathbf{u}h)}{\partial t}\right)\,, \tag{2}$$

$$\frac{\partial (vh)}{\partial t} + \nabla \cdot ((vh)\mathbf{u}) = -g'h\frac{\partial \eta}{\partial y} - fuh + \frac{H^2}{6}\frac{\partial}{\partial y}\left(\nabla \cdot \frac{\partial (\mathbf{u}h)}{\partial t}\right)\,, \tag{3}$$

where $\mathbf{u} = (u(x,y,t), v(x,y,t))$ is the velocity field, $h(x,y,t) = H(x,y) + \eta(x,y,t)$ is the total layer thickness with H representing the undisturbed layer thickness, and η is the interface displacement. Here we use the system (1)-(3) as a simple model of the baroclinic mode for a two-layer fluid with upper and lower layer densities of ρ_1 and ρ_2, respectively. The constants $g' = g(\rho_2 - \rho_1)/\rho_2$ and f are reduced gravity and the Coriolis frequency, respectively. The difference between the set of equations (1)–(3) and the traditional shallow water model is the inclusion of the dispersive terms $\frac{H^2}{6}\nabla(\nabla \cdot (\mathbf{u}h)_t)$ found in the momentum equations (2) & (3). The above system was first proposed by Brandt et al. (1997) in their study of internal waves in the Strait of Messina. This system is derived by a perturbation expansion in powers of the small dimensionless parameter $\mu = (H/L)$, and therefore is only physically relevant if $\mu \ll 1$.

In this study, we rewrite the system (1)-(3) in non-conservative form and in standard polar coordinates $(r,\theta) \in [r_{min}, r_{max}] \times [0, 2\pi]$. The mixed space/time derivatives are removed from the system be introducing the auxiliary scalar variable $z = \nabla \cdot \mathbf{u}_t$ and deriving an elliptic equation for z by taking the divergence of the momentum equations as was done by Eskilsson and Sherwin (2005) who solved a similar system of equations with the discontinuous Galerkin finite element method (DG-FEM). The resulting augmented system is

$$\frac{\partial h}{\partial t} + \frac{1}{r}\left(\frac{\partial (rhu_r)}{\partial r} + \frac{\partial (hu_\theta)}{\partial \theta}\right) = 0\,, \tag{4}$$

$$\frac{\partial u_r}{\partial t} = a_r + \gamma\frac{\partial z}{\partial r}\,, \tag{5}$$

$$\frac{\partial u_\theta}{\partial t} = a_\theta + \frac{\gamma}{r}\frac{\partial z}{\partial \theta}\,, \tag{6}$$

$$\nabla\gamma \cdot \nabla z + \gamma\nabla^2 z = \nabla \cdot \mathbf{a}\,, \tag{7}$$

with

$$\nabla = \hat{\mathbf{r}}\frac{\partial}{\partial r} + \hat{\boldsymbol{\theta}}\frac{1}{r^2}\frac{\partial^2}{\partial \theta^2}\,,\ \nabla^2 = \frac{1}{r}\frac{\partial}{\partial r}r\frac{\partial}{\partial r} + \frac{1}{r^2}\frac{\partial^2}{\partial \theta^2}\,, \tag{8}$$

$$\nabla \cdot \mathbf{a} = \frac{1}{r}\left(\frac{\partial (ra_r)}{\partial r} + \frac{\partial a_\theta}{\partial \theta}\right)\,, \tag{9}$$

$$\mathbf{a} = a_r\hat{\mathbf{r}} + a_\theta\hat{\boldsymbol{\theta}}\,, \tag{10}$$

$$a_r = -g'\frac{\partial \eta}{\partial r} + fu_\theta - u_r\frac{\partial u_r}{\partial r} - \frac{u_\theta}{r}\frac{\partial u_r}{\partial \theta} + \frac{u_\theta^2}{r}\,, \tag{11}$$

$$a_\theta = -\frac{g'}{r}\frac{\partial \eta}{\partial \theta} - fu_r - u_r\frac{\partial u_\theta}{\partial r} - \frac{u_\theta}{r}\frac{\partial u_\theta}{\partial \theta} - \frac{u_r u_\theta}{r}\,, \tag{12}$$

where $\gamma = H^2/6$ is, in general, allowed to vary in space, and u_r and u_θ are the radial and annular velocities, respectively.

The system is discretized in space using a Fourier pseudospectral method in the annular direction and a Chebyshev pseudospectral method in the radial direction. In our simulations we always take $r_{min} > 0$ to avoid the singularity and undesired clustering of grid points near $r = 0$ that are associated with the standard polar coordinates mapping.
The boundary conditions imposed are reflective wall conditions at the inner and outer radii of the basin:

$$u_r = 0 \quad \text{at} \quad r = r_{min}, r_{max} \ , \tag{13}$$

$$\frac{\partial \eta}{\partial r} = 0 \quad \text{at} \quad r = r_{min}, r_{max} \ . \tag{14}$$

Fourier and Chebyshev differentiation are implemented with the Fast Fourier Transform (FFT) for speed and memory efficiency. The elliptic problem (7) is solved iteratively with the generalized minimum residual method (GMRES) using the LU-factorization of the second-order finite difference operator as a preconditioner in order to reduce the iteration count to a reasonable number. For a discussion of GMRES and pre-conditioning, see Trefethen and Bau (1997).

The temporal discretization was carried out with the second-order accurate Leapfrog method. A spatial wavenumber cut-off filter, similar to that used by Hesthaven and Warburton (2008) for the DG-FEM method, of the form

$$\sigma(k) = \begin{cases} 1, & 0 \le k < k_{crit} \\ \exp\left(\alpha \left(\frac{k-k_{crit}}{k_{max}-k_{crit}}\right)^s\right), & k_{crit} \le k \le k_{max} \end{cases} \tag{15}$$

was used in both r and θ directions during time-stepping to prevent aliasing errors from driving weak numerical instabilities. The parameters α, s, and k_{crit} are tunable and, in general, their values must be determined through experimentation. In the results presented in this paper, we use $k_{crit} = 0.15 k_{max}$, $s = 4$, $\alpha = \ln 10^{-12}$, where k_{max} is the Nyquist wavenumber.

3. Results and Discussion

The physical parameters were chosen such that the idealized circular basin would be similar to the physical situation of Lake Kinneret, Israel by inferring approximate values from the data presented in Saggio and Imberger (2001). To that end, the physical parameters in all simuations were chosen (unless otherwise indicated) as follows: $r_{max} = 8435$ m, $r_{min} = 1$ km, $g' = 0.024525$ ms^{-2} , $H = 12.8$ m, $f = 7.8828 \times 10^{-5}$ s^{-1}. Under these parameters, the Rossby deformation radius is $L_D = \sqrt{g'H}/f = 7107$ m, which is quite similar to the distance between the inner and outer basin radii.

In all cases, the initial conditions are taken to be

$$\eta_0 = \eta(r, \theta, t = 0) = \eta_0^{max} \, \mathrm{e}^{-10^{-7}(r-r_{max})^2 - 50\left(\theta - \frac{\pi}{2}\right)^2} \ , \tag{16}$$

$$u_{\theta,0} = u_\theta(r, \theta, t = 0) = \sqrt{\frac{g'}{H}} \eta_0 \ , \tag{17}$$

$$u_{r,0} = 0 \ , \tag{18}$$

reflecting a coastally localized interfacial perturbation propagating in the annular direction at the long internal wave speed $\sqrt{g'H}$. This relation between u_θ and η is inspired from the linear Kelvin wave solution that can be derived assuming that the radial pressure gradient and annular velocity are in geostrophic balance. For simplicity, however, the 'Rossby radius' decay scale L_D is ommitted from the initialization.

3.1. Effect of nonlinearity

In Figures 1 and 2 the maximum amplitude of the initial distrubance was taken to be $0.01H$ and $0.25H$, respectively to illustrate the effect of nonlinearity on a coastally-propagating wave in a lake similar to Lake Kinneret.

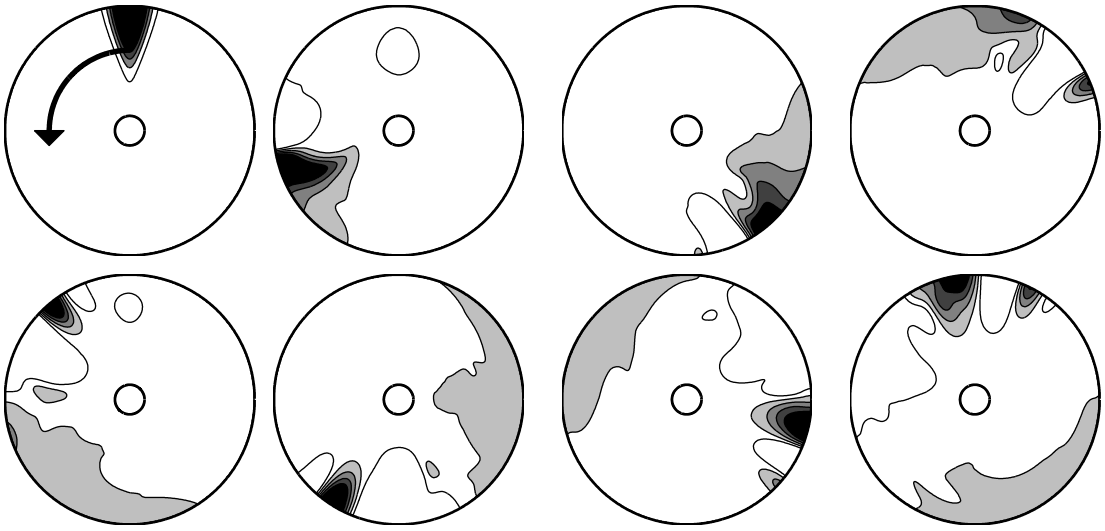

Figure 1: Evolution of an initial interfacial perturbation propagating in the counter-clockwise longshore direction. Snapshots were taken at $t = 0, 7, 14, 21$ h (top) and $t = 28, 35, 42, 49$ h (bottom). The maximum amplitude of the perturbation was taken to be $\eta_0^{max} = 0.01H$. The contour interval is given by five equally spaced values between $-0.03\,\eta_0^{max}$(white) and $0.375\,\eta_0^{max}$(black).

In Figure 1, the effects of nonlinearity are negligible, and as a result no steepening occurs. By $t = 14$ h, the initial shape of the disturbance has spread out considerably and a region of interfacial depression follows the primary elevation wave. By $t = 28$ h, the region behind the depression has become the highest point of interfacial elevation, and the region of largest amplitude. This process of the wavefront losing energy to the interior of the basin by long Poincaré waves continues throughout the evolution. At subsequent times, the resulting wave field is best described as a nearly basin-scale wavefront followed by an undular tail, with the wavelength decreasing towards the rear of the tail.

In Figure 2, the effects of nonlinearity play a key role in the evolution of the wave field. By $t = 7$ h, the initial disturbance has steepened up to a near shock. However, the formation of the shock is prevented by the dispersive terms in equations (2)-(3). When nonlinear steepening and dispersion are in balance, a collection of high-frequency solitary-like waves can be observed in the wave field; however, this is difficult to discern in Figure 2. When the flow is animated, it appears that two-dimensional interactions between the solitary-like waves occur, and that they lose energy by interacting with the interior of the basin. As in the linear case (Figure 1), the elevation at the front of the wave eventually

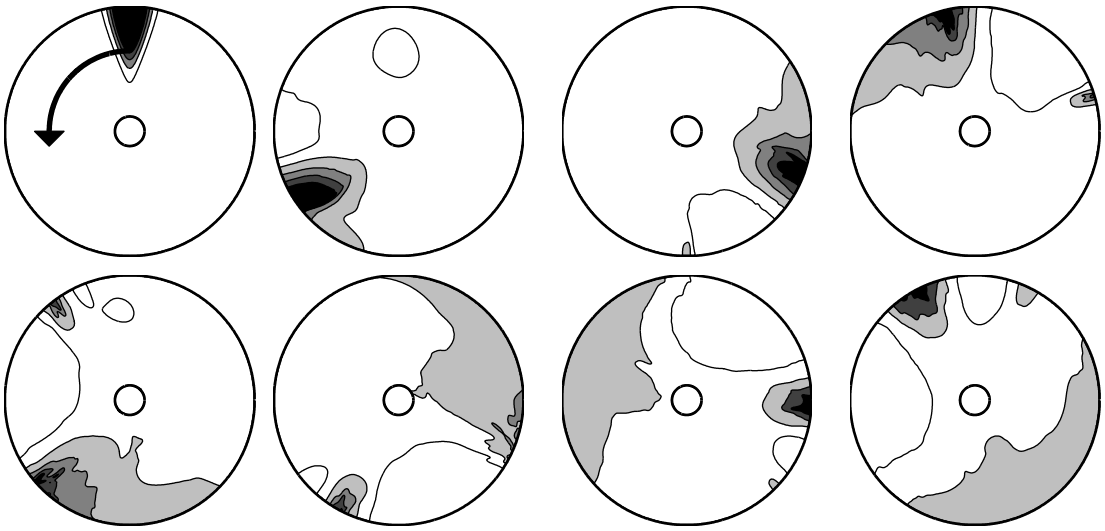

Figure 2: Like Figure 1, but with $\eta_0^{max} = 0.25H$.

spreads sufficiently such that the elevated region behind the interfacial depression becomes the region of largest amplitude in the basin. After sufficient time has passed, solitary-like waves can be found in this region of elevation due to nonlinear steepening, and the process continues.

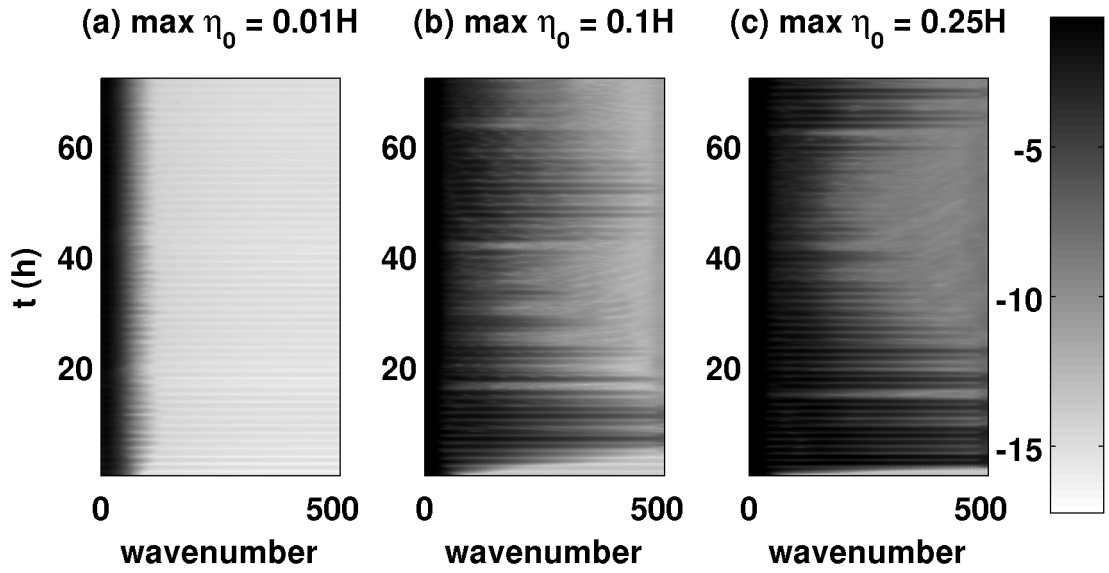

Figure 3: Evolution of $\log_{10}$ of power spectral density (PSD) of η through the slice $r = r_{max}$ for initial interfacial perturbations of maximum amplitudes (a) $0.01H$, (b) $0.1H$, and (c) $0.25H$.

We present space-time plots of the power spectral density (PSD) of the interface displacement at $r = r_{max}$ in Figure 3. The PSD was calculated using the method of windowed overlapping data-sets as explained in Press et al. (2007). The plot illustrates the extent and rate of the nonlinear steepening for initial disturbances of maximum amplitudes of $0.01H$, $0.1H$, and $0.25H$. In the linear case, ($\eta_0^{max} = 0.01H$) the PSD is nearly constant in time. In the cases where $\eta_0^{max} = 0.1H, 0.25H$, energy is quickly spread to the shortest length-scales available, and the two ensuing PSD evolutions are very similar.

Not surprisingly, the cascade to small-scales occurs fastest in the most nonlinear case ($\eta_0^{max} = 0.25H$). This result provides insight into the importance of nonlinear steepening in the link between low-frequency and high-frequency internal waves.

3.2. Effect of rotation

We now turn our attention to the effects of f-plane rotation on the evolution of the wavefield for an initial interfacial perturbation of fixed amplitude. In Figure 4, f is increased to 1.4544×10^{-4} s^{-1}, reflecting the Coriolis frequency at the North Pole, the highest value of f possible on Earth. In this case, the Rossby deformation radius is $L_D = 3852$ m, or about half-way between the inner and outer basin radii.

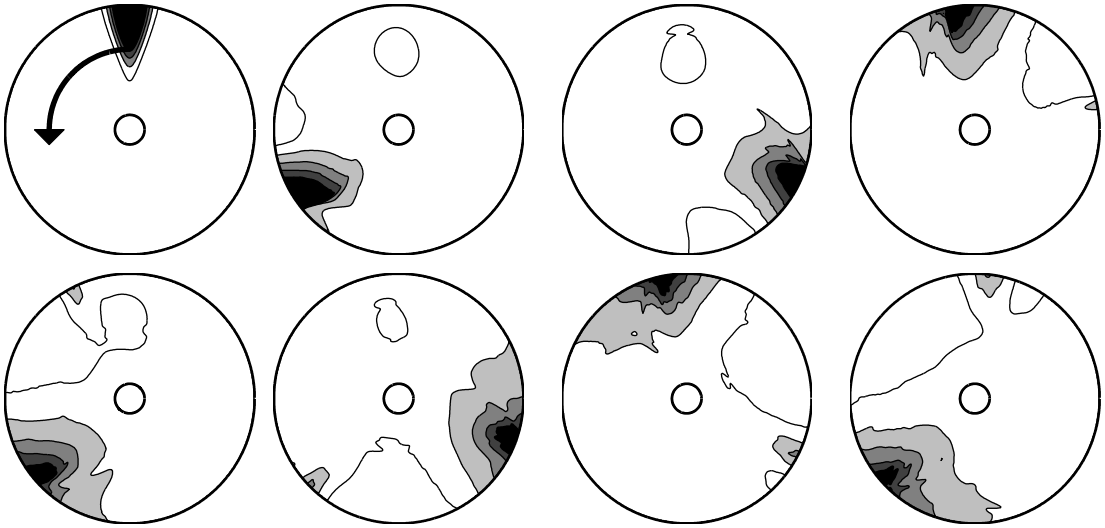

Figure 4: Like Figure 1, but with $\eta_0^{max} = 0.25H$ and $f = 1.4544 \times 10^{-4}$ s^{-1}.

Due to the linear analysis performed by Stocker and Imberger (2003), we expect increasing f to result in the strengthening of the linear Kelvin mode, thereby weakening the interactions between our coastally propagating disturbance and the interior of the basin. Indeed, this effect can be found in our results in two main observations: firstly, it is found that the length of time required for the primary wavefront to lose energy to its tail is increased substantially when compared to Figure 2; and secondly, the outward spreading of the intial disturbance to near basin scales takes considerably longer. Both of these effects are attributable to the relative strengthening of the Kelvin mode compared to the corresponding free Poincaré modes predicted by linear theory. This result may also be interpreted in terms of the Rossby deformation radius, L_D: a smaller value of L_D lowers the effect of boundary curvature, leading to a scenario more akin to a Kelvin wave propagating along a straight coastline (see Section 3.3), hence there are less radiating Poincaré waves.

In Figure 5, the Coriolis parameter was switched off, $f = 0$ s^{-1}. Since rotation is neglected, there is no coastal trapping mechanism (Kelvin mode), and all long waves are expected to propagate with speed $\sqrt{g'H}$. Although the evolution is somewhat similar to the case shown in Figure 2 (where $f = 7.8828 \times 10^{-5}$ s^{-1}), a key observation is that the main wave front loses energy to its undular tail more rapidly in the case with $f = 0$ s^{-1}.

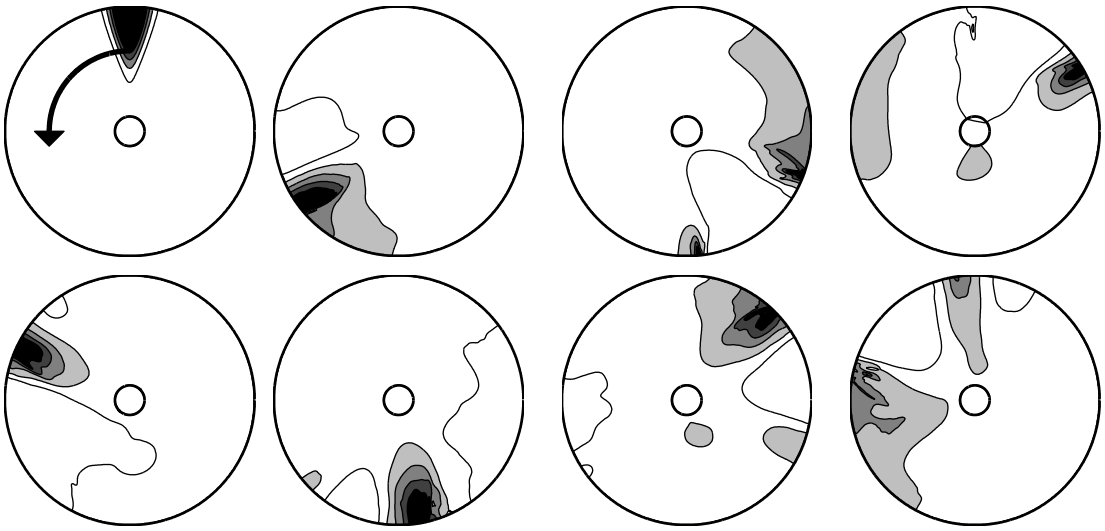

Figure 5: Like Figure 1, but with $\eta_0^{max} = 0.25H$ and $f = 0\ \mathrm{s}^{-1}$.

This observation reflects that the opposite effect to that shown in Figure 4 is occurring. Namely, that the Poincaré wave portion of the linear solution spectrum is at maximum strength relative to the Kelvin wave, which by definition, is not present in this case.

3.3. Results in a channel

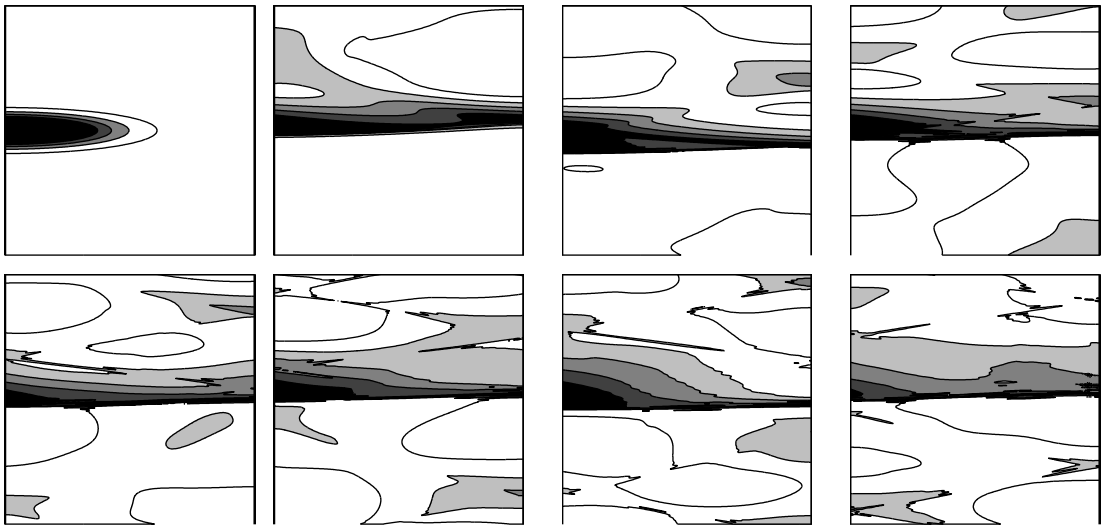

Figure 6: Evolution of an initial free surface perturbation propagating in the southward longshore direction in a periodic channel. Snapshots were taken at $t = 0, 7, 14, 21$ h (top) and $t = 28, 35, 42, 49$ h (bottom) in a reference frame centered about the point of maximum interfacial displacement. The maximum amplitude of the initial perturbation was taken to be $\eta_0^{max} = 0.25H$.

As a final comment, we present a case analogous to that presented in Figure 2 ($f = 7.8828 \times 10^{-5}\ \mathrm{s}^{-1}$, $\eta_0^{max} = 0.25H$), but we have replaced the circular geometry with a periodic meridional channel. The channel's width was set to 8435 m and its length to $2\pi \times 8435$ m (note that the aspect ratio is not reflected in Figure 6). The initial disturbance

was localized along the western coastline, and initialized to propagate southwards, which is consistent with the classical linear Kelvin wave solution.

The resulting evolution, shown in Figure 6, is similar to what one expects given the results presented in Figure 2. A key difference is that Poincaré waves radiating across the channel allow southward propagating coastal waves to form on the *eastern* side of the basin. These waves must consist purely of Poincaré mode components, because a Kelvin wave along the east coast is required to propagate northward since Kelvin waves are well-known to be right-bound in the northern hemisphere, where $f > 0$ (see Gill (1982)). Another important observation is that the wave front does not spread forward as it does in the case of a circular basin, implying that such effects are a result of boundary curvature. Other main features of the circular case, such as the emergence of solitary-like waves and the formation of an undular tail, remain intact in the channel geometry.

References

Boyd, J. (2001). *Chebyshev and Fourier Spectral Methods*. Dover Publications, 2nd edition.

Brandt, P., Rubino, A., Alpers, W., and Backhaus, J. (1997). Internal waves in the Strait of Messina Studied by a numerical model and synthetic aperture radar umages from *ERS 1/2* Satellites. *J. Phys. Oceangr.*, 27:648–663.

de la Fuente, A., Shimizu, K., Imberger, J., and Niño, Y. (2008). The evolution of internal waves in a rotating, stratified, circular basin and the influence of weakly nonlinear and nonhydrostatic accelerations. *Limnol. Oceanogr.*, **53**(6):2738–2748.

Eskilsson, C. and Sherwin, S. (2005). Spectral/*hp* discontinuous Galerkin methods for modelling 2d Boussinesq equations. *J. Sci. Comp.*, 22:269–288.

Gill, A. (1982). *Atmosphere-Ocean Dynamics*. Academic Press, 1st edition.

Hesthaven, J. and Warburton, T. (2008). *Nodal Discontinuous Galerkin Methods*. Springer.

Press, W., Teukolsky, S., Vetterling, W., and Flannery, B. (2007). *Numerical Recipes*. Cambridge University Press, 3rd edition.

Saggio, A. and Imberger, J. (2001). Internal wave weather in a stratified lake. *Limnol. Oceanogr.*, 43:1780–1795.

Stocker, R. and Imberger, J. (2003). Energy partitioning and horizontal dispersion in a stratified rotating lake. *J. Phys. Oceanogr.*, 33:512–529.

Tomasson, G. and Melville, W. (1992). Geostrophic adjustment in a channel: nonlinear and dispersive effects. *J. Fluid Mech.*, 241:23–48.

Trefethen, L. (2000). *Spectral Methods in MATLAB*. Society for Industrial and Applied Mathematics.

Trefethen, L. and Bau, D. (1997). *Numerical Linear Algebra*. Society for Industrial and Applied Mathematics.